Supporting Information

Comparison of the Arrhenius Parameters Between Conventional Hydrothermal and Microwave-Assisted Synthesis Methods for Tin Oxide Nanoparticles

Morgan Chen,[a] Laura Glei Graversen, [b] Sanjit Ghose,[c] Kirsten M. Ø. Jensen,[b] B. Reeja-Jayan [a]

Pair Distribution Function (PDF) Analysis

The 2D diffraction data was azimuthally integrated with the Fit2D software to obtain 1D diffraction intensities.[1] The PDF data processing was performed using PDFgetX3 within the xPDFsuite software to subtract out the signal from the background and to set the Fourier transformation limits (see Fig. 2).[2]–[4] The experimental PDF, or $G(r)$, given by:

$$G(r) = \frac{2}{\pi}\int_{Q_{min}}^{Q_{max}} F(Q)\sin(Qr)dQ$$

where $F(Q)$ is the background-subtracted, corrected, and normalized reduced structure function, Q is the scattering momentum transfer, and *r* is the interatomic distance between atoms.

The data was transformed with Q_{min} = 0.5 Å^{-1} and Q_{max} = 17.5 Å^{-1}. Structural refinements and analysis were conducted using PDFgui [5].[5] The instrument resolution parameters Q_{damp} and Q_{broad} are refined when fitting the standard CeO_2 data, and are fixed in the subsequent structural refinements of PDF data, where Q_{damp} = 0.0307 Å^{-1} and Q_{broad} = 0.0478 Å^{-1}.[5][6] Least-square refinements were performed by minimizing the fit residual between the structural model and the experimental data, quantified by the goodness-of-fit R_w, which is defined as:

$$R_w = \sqrt{\frac{\sum_{i=1}^{N}[G_{obs}(r_i) - G_{calc}(r_i;P)]^2}{\sum_{i=1}^{N} G_{obs}^2(r_i)}}$$

where G_{obs} is the PDF of the experimental data, G_{calc} is the PDF calculated from the structure model, and P is the set of refinable parameters used in the structure model. Lower values of R_w represent a higher-quality match between the experimental PDF and the refined model PDF.

Table S1. PDF refinement results for the final SnO_2 nanoparticles from conventional hydrothermal and microwave-assisted synthesis conditions. The lower final yield from the microwave-assisted synthesis conditions resulted from premature vessel rupture during nanoparticle growth due to autogenous pressure buildup and did not affect the extraction of rate constants that provided the relevant Avrami and Arrhenius parameters.

	Conventional (164 ºC)	Conventional (174 ºC)	Conventional (181 ºC)	Microwave (130 ºC)	Microwave (138 ºC)	Microwave (143 ºC)
SnO_2 Phase Scale Factor	0.172	0.296	0.208	0.169	0.220	0.149
$[SnCl_4(H_2O)_2]\cdot H_2O$ Phase Scale Factor	1.82	1.04	1.67	1.62	3.30	4.04
SnO_2 Mass (relative)	0.070	0.201	0.095	0.081	0.054	0.030
$[SnCl_4(H_2O)_2]\cdot H_2O$ Mass (relative)	0.930	0.799	0.905	0.919	0.946	0.970
a (Å)	4.77	4.76	4.76	4.76	4.76	4.76
c (Å)	3.19	3.18	3.19	3.19	3.19	3.19
Sn U_{iso} ($Å^2$)	0.005	0.006	0.005	0.005	0.006	0.006
O U_{iso} ($Å^2$)	0.042	0.040	0.048	0.039	0.028	0.041
δ_1	1.64	2.77	1.58	1.69	1.53	1.85
Nanoparticle Diameter (Å)	38.5	49.0	44.5	38.1	38.7	41.2
R_w	0.284	0.204	0.274	0.289	0.209	0.209

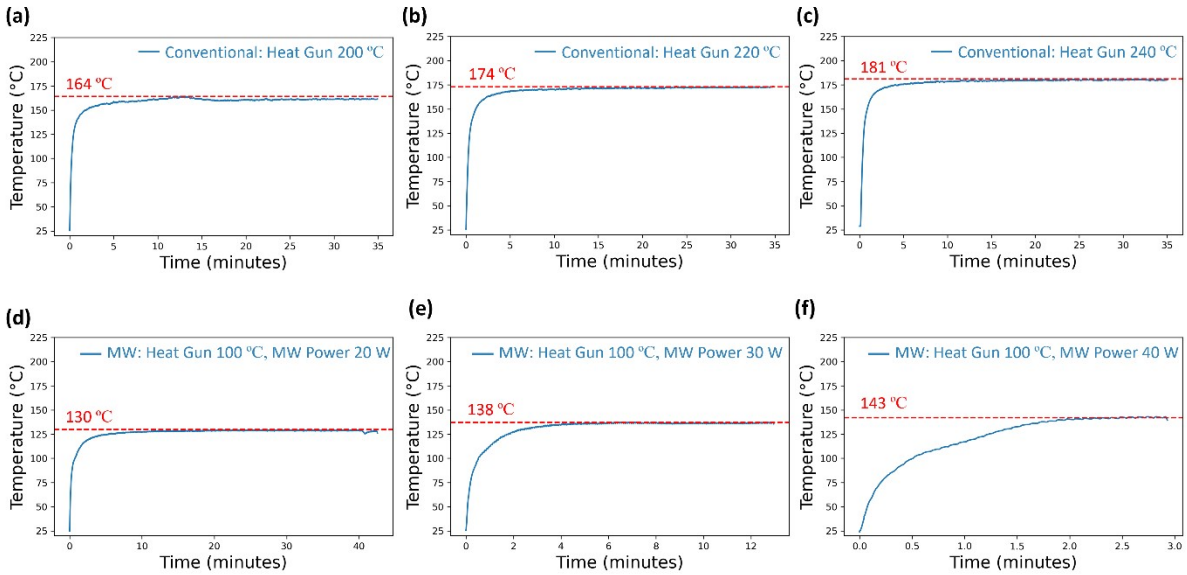

Figure S1. Plots of the measured steady state or maximum temperatures of the reaction tube at the various MW and conventional synthesis conditions. (a) The temperature profile of the conventional synthesis condition with a heat gun output temperature at 200 ºC. (b) The temperature profile of the conventional synthesis condition with a heat gun output temperature at 220 ºC. (c) The temperature profile of the conventional synthesis condition with a heat gun output temperature at 240 ºC. (d) The temperature profile of the MW-assisted synthesis condition with a heat gun output temperature at 100 ºC and a pulsed MW power of 20 W. (e) The temperature profile of the MW-assisted synthesis condition with a heat gun output temperature at 100 ºC and a pulsed MW power of 30 W. (f) The temperature profile of the MW-assisted synthesis condition with a heat gun output temperature at 100 ºC and a pulsed MW power of 40 W.

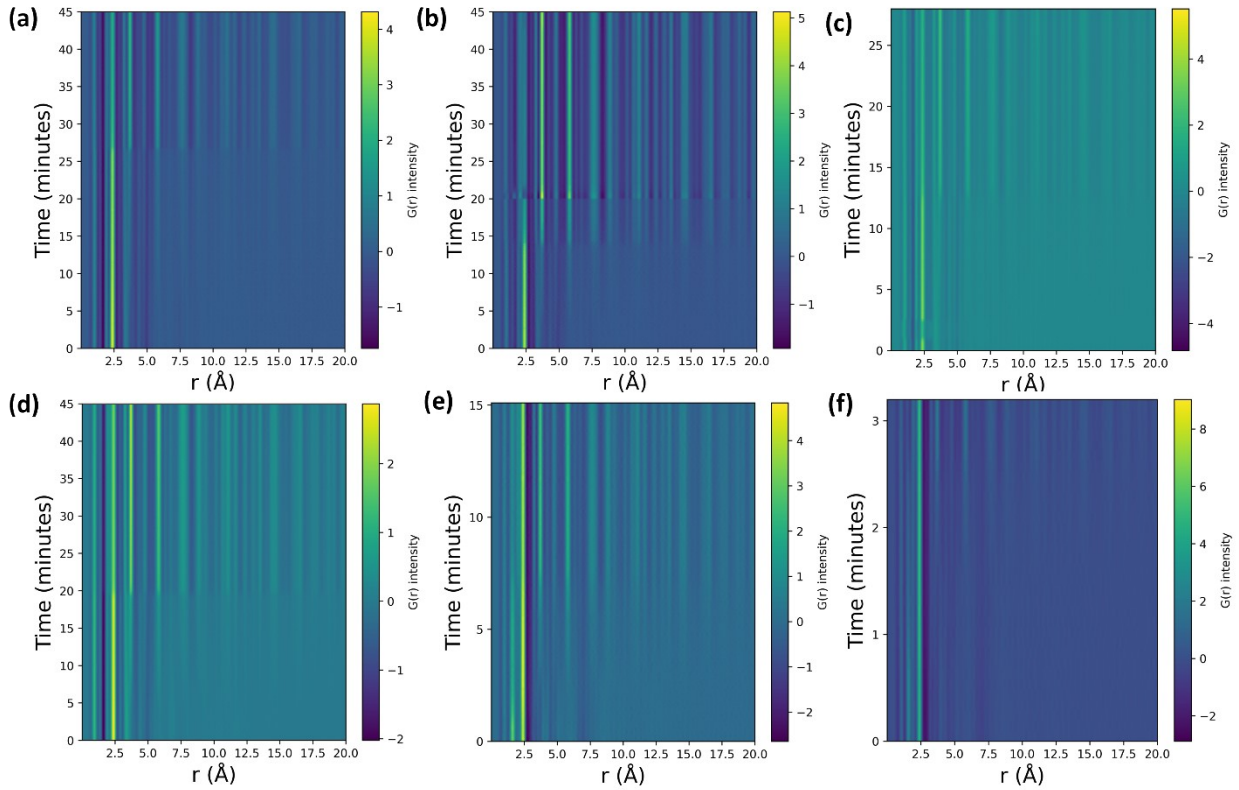

Figure S2. The in-situ PDF plots from the various MW and conventional synthesis conditions. (a) Time-resolved map of the in-situ PDFs corresponding to the conventional hydrothermal synthesis of SnO2 nanoparticles at 164 ºC. (b) Time-resolved map of the in-situ PDFs corresponding to the conventional hydrothermal synthesis of SnO2 nanoparticles at 174 ºC (c) Time-resolved map of the in-situ PDFs corresponding to the conventional hydrothermal synthesis of SnO2 nanoparticles at 181 ºC. (d) Time-resolved map of the in-situ PDFs corresponding to the MW-assisted hydrothermal synthesis of SnO2 nanoparticles at 130 ºC. (e) Time-resolved map of the in-situ PDFs corresponding to the MW-assisted hydrothermal synthesis of SnO2 nanoparticles at 138 ºC. (f) Time-resolved map of the in-situ PDFs corresponding to the MW-assisted hydrothermal synthesis of SnO2 nanoparticles at 143 ºC.

Table S2. Resultant fit parameters from Avrami modeling for conventional hydrothermal and microwave-assisted synthesis.

	Conventional (164 ºC)	Conventional (174 ºC)	Conventional (181 ºC)	Microwave (130 ºC)	Microwave (138 ºC)	Microwave (143 ºC)
k (min^{-1})	0.433	0.482	0.511	0.407	0.459	6.59
n	0.72	0.57	0.61	0.61	1.26	1.19
R^2	0.947	0.883	0.962	0.948	0.976	0.992

Table S3. Resultant fit parameters and statistics from Arrhenius plots for conventional hydrothermal and microwave-assisted synthesis. The values determined for the microwave-assisted synthesis condition are shown in the first column labeled accordingly. The values determined for the microwave-assisted synthesis condition using only the experimentally accessible isothermal conditions is shown in the next column. The uncertainty quantification for this column is insignificant as a consequence of having only two data points. Therefore, the values should be interpreted with caution. The values determined for microwave-assisted synthesis conditions for hypothetical steady-state temperatures above the measured maximum of 143 ºC in the third data point (to account for higher reaction temperatures due to local heating phenomena) are shown in the following columns. Regardless of the circumstances, the cases trend toward an elevated pre-exponential factor.

	Conventional	Microwave (presented)	Microwave (only steady-state data)	Microwave (third data point at 193 ºC)	Microwave (third data point at 243 ºC)
Slope (K)	-1945	-32570	-2490	-8640	-5229
Y-intercept	3.617	79.51	5.28	20.40	12.01
R^2	0.9968	0.6564	1	0.9909	0.9982
Standard Error for Slope	109.8	23560	0	826.4	220.7
Standard Error for Y-intercept	0.2463	57.48	0	1.949	0.5070
Apparent Activation Energy, E_a (kJ mol^{-1})	16.17	270.8	20.70	71.83	43.47
Apparent Pre-Exponential Factor, A (min^{-1})	37.22	3.401E+34	196.0	7.26E+8	1.65E+5
Standard Error for E_a (kJ mol^{-1})	±0.9127	±195.9	0	±6.871	±1.835
Standard Error for A (min^{-1})	±9.165	±1.956E+36	0	±1.415E+9	±8.359E+4

References

[1] A.P. Hammersley, S.O. Svensson, M. Hanfland, A.N. Fitch, D. Hausermann, *High Pressure Research* **1996**, *14*, 235.
[2] X. Yang, P. Juhas, C.L. Farrow, S.J.L. Billinge, **2015**.
[3] P. Juhás, T. Davis, C.L. Farrow, S.J.L. Billinge, *J Appl Crystallogr* **2013**, *46*, 560.
[4] P.F. Peterson, E.S. Božin, T. Proffen, S.J.L. Billinge, *J Appl Crystallogr* **2003**, *36*, 53.
[5] C.L. Farrow, P. Juhas, J.W. Liu, D. Bryndin, E.S. Božin, J. Bloch, T. Proffen, S.J.L. Billinge, *J. Phys.: Condens. Matter* **2007**, *19*, 335219.
[6] Th. Proffen, S.J.L. Billinge, *J Appl Crystallogr* **1999**, *32*, 572.